# Reducing the hydrogen permeability of steel pipelines by applying internal composite polymer coatings

***A. P. Petkova,*** *Dr. Eng., Prof., Dept. of Materials Science and Technology of Art Products* [1], *e-mail: apetkova@inbox.ru;*
***V. A. Zlotin,*** *Postgraduate Student, Dept. of Materials Science and Technology of Art Products* [1], *e-mail: zlotinvladimir@mail.ru;*
***Ya. E. Gekht,*** *Student, Dept. of Materials Science and Technology of Art Products* [1], *e-mail: jangech95@gmail.com;*
***V. S. Borisova,*** *Student, Faculty of Technology Management and Innovation* [2], *e-mail: vsnikitina2001@gmail.com*
***G. Yu. Kalinin,*** *Dr. Eng., Associate Prof.* [3]

[1] *Empress Catherine II Saint Petersburg Mining University, St. Petersburg, Russia*
[2] *ITMO University, St. Petersburg, Russia*
[3] *National Research Center "Kurchatov Institute" - Central Research Institute of Structural Materials "Prometey", St. Petersburg, Russia*

The paper considers the possibility of using composite polymer-metal coatings to reduce water permeability. Coatings including modified fluoroplastic enamel (MFPE) and aluminum have been prepared and tested. The aluminum coating was applied by cold gas-dynamic spraying. MFPE was modified to increase the adhesion and crosslinking density of the coating using carbon nanotubes, SiC, h-BN nanoparticles, and a photoinitiator 819 for UV curing. The Devanathan-Stachurski method was used as a method for estimating hydrogen diffusion through a coated metal. Graphite coating was used for testing polymer coatings, which was also separately tested for hydrogen permeability. The diffusion coefficients and the diffusion flow of hydrogen through steel with and without coatings have been experimentally determined. The reduction coefficients and efficiency of reducing the diffusion and diffusion flow of hydrogen are determined for the coatings. It was found that MFPE /Al coatings can ensure the effectiveness of reducing diffusion by 87.7 % and diffusion flow by 77.1 %. For MFPE, these values were 68.8 % and 67 %, respectively, and for graphite – 52.1 % and 57.4 %, respectively. The determining influence on the protective properties of a fluoroplastic coating is exerted by the type of nano-additives (SiC or h-BN) and their ability to distribute evenly, where the best combination is CNT with SiC with the maximum ratio of diffusion reduction coefficients 89.5 % and permeability 86.8 %. The patterns identified for fluoroplastic compounds are fully preserved on coatings with an adhesive layer of Al+AlOOH, which increases the coating thickness and increases the effectiveness of diffusion reduction for all formulations, including CNTs with SiC up to 97 % and diffusion flux up to 89.3 %. The possibility of using a composite coating for in-tube coatings during additional testing is proposed.
***Key words:*** hydrogen permeability, hydrogen diffusion, composite coatings, fluoroplastic, aluminum.
***DOI:*** 10.17580/cisisr.2026.01.15

## Introduction

At present time, development of production, transportation and storage of energy resources plays especial role in the national economical sovereignty [1]. The most part of the researches in this field is devoted to hydrocarbon energy sources [2–4], however, their use leads to atmosphere pollution. Hydrogen is now considered as an ecological and energy effective alternative [5, 6]. At the same time, there are several problems which restrict hydrogen use, because hydrogen is characterized by high permeability in materials due to its small atomic radius, what leads to hydrogen embrittlement and lowering of mechanical properties of these materials [7–9].

Today there is no common criterion for assessment of materials resistance to hydrogen embrittlement. Natural testing is durable, while accelerated testing provides controversial results for the methods of hydrogen generation [10]. The researches are divided in two directions: varying of mechanical properties during hydrogenation [11–13] and study of hydrogen diffusion through material [14–16], what is important for assessment of protective coatings. Many works are devoted to internal coatings in tubes [17–19]. Polymers themselves are insufficiently resistant for hydrogen penetration owing to their porosity, but additives (metal oxides, graphene, nanotubes) compact the structure and make diffusion ways more complicated [20]. Adhesion of coating to steel is important, because hydrogen conglomeration along a boundary can lead to delamination. Application of metals with low permeability (Al, Cu, Ni [21–23]) via gas dynamic spraying, electrochemical deposition and applying diffusion coatings [24] is another approach, but complication of surface control restricts their use inside tubes. Combination of spraying methods for metal coating with consequent heat treatment and application of a polymer layer is also prospective. It is also possible to use compositions on the base of epoxy resin [25] or fluoroplastic [26] as potential polymer

coatings inside tubes; fluoroplastic has low permeability among polymers [27].

The most part of researchers consider graphene as a modifying additive [28–30], as well as carbides and nitrides of several elements (e. g. boron nitride) [30]. However, use of carbon nanotubes is examined insufficiently [31], though they are more acceptable material in comparison with graphene. It is suitable for application in larger scale (e. g. for internal tube coatings), and they are characterized by smaller size in comparison with carbides and nitrides of different elements, what allows filling of a polymer matrix more compactly. It also should be noted that adding nanotubes in a coating improves its adhesion [32]. Today there were no researches conducted, which are devoted to assessment of barrier properties of aluminium-polymer composition with photo-cured fluoroplastic coatings, that were modified by carbon nanotubes and nano-additives SiC or h-BN.

The aim of this research is assessment of effectiveness of hydrogen diffusion reducing through steel 20 during applying a composite aluminium-polymer coating. Aluminium was chosen owing to its low water permeability [33, 34]; its processing makes it possible to form AlOOH layer [35], which improves adhesion and reduces diffusion. Fluoroplastic, which was modified by carbon nanotubes and nano-additives SiC or h-BN, was used as polymer coating. To conduct the experiment via Devanathan-Stachurski method, graphite lacquer providing conductivity was applied on polymer layers.

## Materials and methods of the research

The samples for testing were fabricated from sheet steel 20 with length and width 60 × 90 mm and with thickness about 3.8 mm. Part of these samples were ground and polished to get a mirror surface for testing without coating, while for coating application, surface of the samples was subjected to sandblasting with obtaining roughness Ra ~5–5.5 μm.

To decrease steel water permeability, three types of coatings were used: graphite lacquer (GL) on epoxy base, modified fluoroplastic enamel (MFPE) composition with graphite and three-layered metal-polymer coating Al+AlOOH+MFPE+GL. Aluminium layer was applied by cold gas-dynamic spraying, then the samples were purified by ultrasonic in acetone and were held in boiling water to form the hydrated AlOOH layer. To prepare polymer coatings, fluoroplastic enamel FP-566 was used, it had additives of carbon nanotubes (0.5 %), photoinitiator Irgacure 819 (0.5 %), nano-additives SiC or h-BN (each 0.5 %) and butyl acetate. The mixture was dispersed by ultrasonic and applied by spraying. The average layer thickness was 70–80 μm, and a thin graphite layer (~5 μm) was applied to provide electric conductivity. Thickness of the lacquer layer was increased to 40 μm for its direct testing.

Quality assessment of coating application and its structure was carried out using scanning electron microscope and energy dispersion spectrometer (SEM-EDS). To evaluate adhesion strength during hydrogenation, the pull-off test was used (GOST 32299-2025). The tests for hydrogen permeability were carried out in the Devanathan-Stachurski cell with 0.1 M solution of NaOH, graphite electrodes and chlorine-silver electrode for comparison. Hydrogenation current density made 3.75 mA/cm$^2$, operating potential was 200 mV and contact square was equal to 8.04 cm$^2$. The principal operating scheme of a closed circuit in an electrochemical cell is presented in the **Fig. 1**.

Diffusion flow *J(t)* [mol/(s·cm$^2$)] of hydrogen was determined, based on the measured current values in a working electrode depending on time, according to the following formula [36]

$$J(t) = \frac{I(t)}{F \cdot S} \quad (1)$$

where *I(t)* – current at the time *t*, A; *S* – contact square between the surface of a tested sample and working solution, cm$^2$; *F* – Faraday constant, 96485 Kl/mol.

To determine effective diffusion coefficient $D_{eff}$ [cm$^2$/s], the following expression weas used [37–39]:

$$D_{eff} = \frac{h^2}{6 \cdot t_{lag}} \quad (2)$$

where h – total sample thickness, cm ($h = h_s + h_{co}$ for coated samples, where $h_s$ – sample thickness, cm; $h_{co}$ – coating thickness, cm; $h = h_s$ for non-coated samples), cm; $t_{lag}$ – time moment when *J(t)/J(st)* = *I(t)/I(st)* = 0.63, s (**Fig. 2**); *I(st)* current at stationary diffusion ptocedure, A.

The hydrogen diffusion reducing coefficient *DRF* was assessed via experimental curves according to the formula (3), which displays by how many times diffusion reduces owing to coating. Effectiveness of diffusion reducing due to

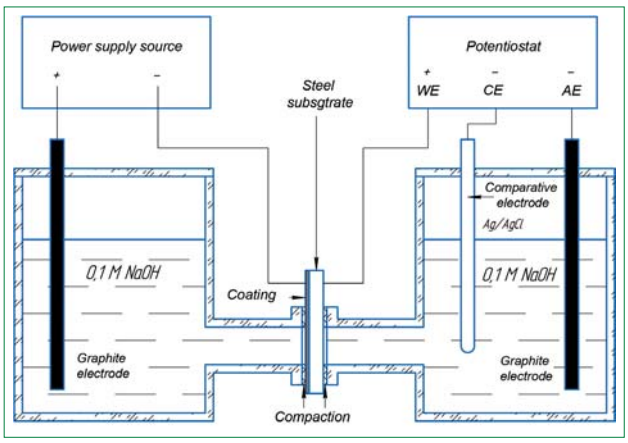


**Fig 1. Scheme of the electrochemical cell:** *WE* – working electrode); *CE* – compara-tive electrode; *AE* – auxiliary electrode

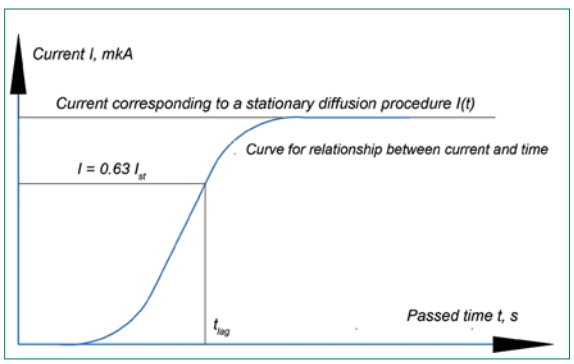


**Fig. 2. Relationship between current at oxidation side and time**

coating is assessed by the coefficient $\eta_D$, % according to the formula (4). The stationary diffusion flow reducing coefficient *JRF* was assessed via experimental curves according to the formula (5), which displays by how many times diffusion flow reduces owing to coating [34]. Effectiveness of diffusion flow reducing due to coating is assessed by the coefficient $\eta_J$, % according to the formula (6).

$$DRF = \frac{D_{\text{eff}}(s)}{D_{\text{eff}}(co)} \quad (3)$$

$$\eta_D = \left(1 - \frac{1}{DRF}\right) \cdot 100\% \quad (4)$$

$$JRF = \frac{J(s)}{J(co)} \quad (5)$$

$$\eta_J = \left(1 - \frac{1}{JRF}\right) \cdot 100\% \quad (6)$$

where $D_{\text{eff}}(s)$, $J(s)$ – diffusion [cm²/s] and diffusion flow [mol/(s·cm²)] of hydrogen through the sample without coating, respectively; $D_{\text{eff}}(co)$, $J(co)$ – diffusion [cm²/s] and diffusion flow [mol/(s·cm²)] of hydrogen through the sample with coating, respectively; $\eta_D$, $\eta_J$ – the effectiveness coefficient of hydrogen diffusion reducing and hydrogen diffusion flow reducing by coating, respectively, %.

## Results and discussion

The results obtained during testing of steel samples without coating and with various coatings are presented in the **Fig. 3** and their processing data is displayed in the **Table 1**.

Assessment of effectiveness of hydrogen flow and diffusion reducing by coatings id conducted on the base of analysis of experimental data and calculations via the formulas (3)–(6). The coating thickness $h_{co}$ was determined as a sum for all layers. Based on the obtained experimental data for the above-mentioned coatings, the following indicators were determined: the hydrogen diffusion reducing coefficient *DRF* (3); the coefficient of effectiveness of hydrogen diffusion reducing due to coating $\eta_D$ (4); the stationary diffusion flow reducing coefficient *JRF* (5); the coefficient of effectiveness of stationary diffusion flow reducing due to coating $\eta_J$ (6).

The value of effectiveness for each type of coatings is located within the range confirmed by technical literature (~50–90 %) [17, 28]. Graphite coating with $\eta_J$=52.1 % is not effective for reducing of hydrogen diffusion flow. It can be caused by insufficient coating thickness and absence of orientation of graphite ripples, which don't create a crooked path for hydrogen. MFPE+graphite coating with $\eta_J$=68.8 % can be acceptable for the conditions of hydrogen transportation and storage, but it requires finalizing for critical applications. Reducing of a barrier effect due to agglomeration and insufficient dispersion of nanotubes and photoinitiator can be considered as possible causes. Adding more compact and homogenous layers of Al and AlOOH in the third coating allowed effectiveness rising up to 77.7 %, what is suitable for hydrogen transportation in pipelines [28].

The obtained data of effectiveness of hydrogen diffusion coefficient reducing for steel 20 allow clear assessment and comparison of protective properties for each coating. The diffusion coefficient in graphite coating reduces by 67 %, it id rather high effectiveness for a simple graphite coating. In this case, the diffusion coefficient reduces by 57.4 % in modified fluoroplastic coating. Lower adhesion of a fluoroplastic coating (0.31 MPa for tear-off) is considered as a probable cause in comparison with a graphite coating (3.74 MPa for tear-off). When hydrogenation, a coating is gradually exfoliated from the surface due to high hydrogen pressure, what leads to forming of defects between steel a substrate and a coating. Adhesion increase via forming the layer AlOOH (10.1 MPa for tear-off) allowed effectiveness rising up to 87.7 %. Small number of defects inside Al itself and between layers also plays the important role in this case, what is testified by the **Fig. 4** and **Fig. 5**.

Structure of the sample was examined using scanning electron microscopy and energy dispersion spectroscopy (SEM-EDS).

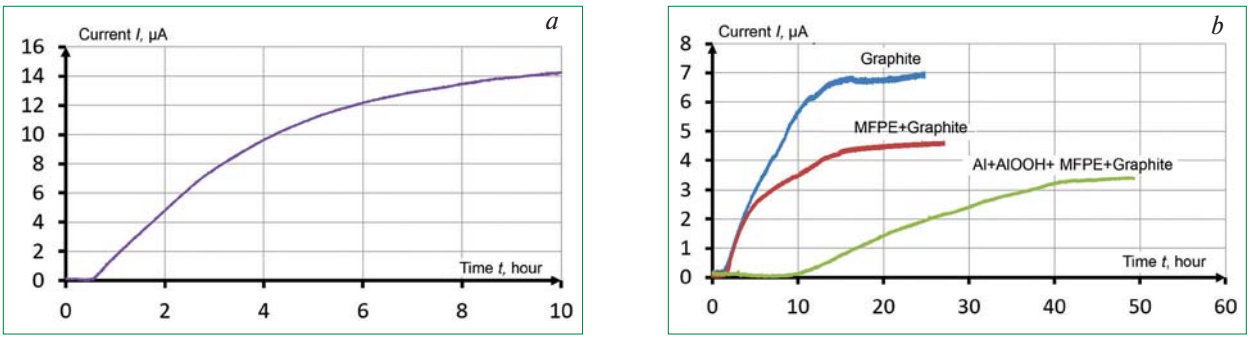


**Fig. 3. The results of testing of steel samples without coating (*a*) and with various coatings (*b*)**

**Table 1. Assessment of effectiveness of protective properties of coatings**

| Sample | $h_{co}$, μm | $h_s$, μm | $D_{\text{eff}} \times 10^6$, cm²/s | $J(t) \times 10^{12}$, mol/(s·cm²) | *DRF* | *JRF* | $\eta_D$, % | $\eta_J$, % |
|---|---|---|---|---|---|---|---|---|
| Steel 20 | – | 3763 | 1.79 | 18.58 | – | – | – | – |
| Steel 20 + GL | 40 | 3803 | 0.591 | 8.89 | 3.03 | 2.09 | 67.0 | 52.1 |
| Steel 20 + MFPE + GL | 76 | 3839 | 0.763 | 5.80 | 2.35 | 3.20 | 57.4 | 68.8 |
| Steel 20+Al-AlOOH+MFPE+GL | 270 | 3980 | 0.22 | 4.25 | 8.14 | 4.37 | 87.7 | 77.1 |

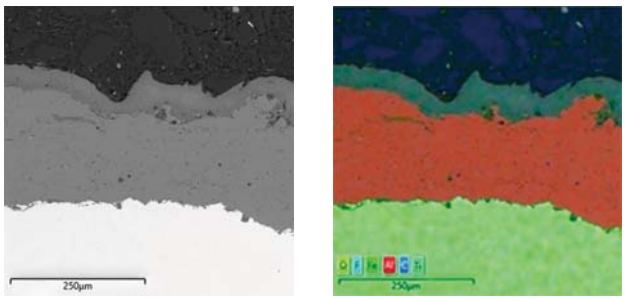


*a* *b*

**Fig. 4. Structure (*a*) and distribution of the elements (*b*) in the coating Al+AlOOH+MFPE+GL**

Aluminium (Al) strip between the steel (Fe) area and fluoroplastic (F) can be clearly seen in the Fig. 4. According to the scale ruler in these figures, thickness of the Al layer really makes up to 250 μm. This layer visually looks rather homogenous by thickness in the examined areas. Distinct separation of phases is observed in the Al chart (Fig. 5, *c*) and Fe chart (Fig 5, *d*). There are no signs of intensive mixing or end-to-end channels from steel to fluoroplastic, avoiding aluminium. It can be seen from the O distribution chart (Fig. 5, *b*) that the most intensive signal is coming not from the total Al layer, but from its external surface which has a boundary with fluoroplastic (Fig. 5, *a*); it testifies on presence of the thin AlOOH layer. It can be seen from these pictures that there is no visible gap between Al layer (with O contour) and fluorine-detecting area (Fig. 4, *b*), what manifests about absence of defects between AlOOH layer and fluoroplastic. Boehmite AlOOH layer forms hydrogen links mainly with fluorine of fluoroplastic (Fig. 5, *a*), not with chemically inert carbon which is completely surrounded by fluorine atoms. Small carbon agglomerates are observed in the fluoroplastic coating itself (Fig. 4, *a*). No direct signs of exfoliation or non-uniformity in the boundary AlOOH/FP-566 were revealed. Fluoroplastic enamel provided well moisturizing and micro-relief filling of a hydrated layer. Titanium Ti (Fig. 5, *e*) is observed in composition of a white pigment inside fluoroplastic coating.

To increase barrier properties of fluoroplastic matrix and to decrease CNT agglomeration, additional dispersion of compositions with nano-additives in an ultrasonic bath during 5 min before spraying and application of 3 layers with UV curing were used. Qualitative assessment of the effect of nano-additives SiC and h-BN on CNT agglomeration in fluoroplastic coating was conducted via scanning electron microscopy (SEM) combined with energy dispersion spectroscopy (EDS) for intensification of phases. The images of modified fluoroplastic coatings with nano-additives CNT, SiC and h-BN and photoinitiator 819, which were obtained during the procedure of back-scattered electrons at voltage 15 kV are presented in the **Fig. 6**. The basic matrix elements are presented by F, pigments $TiO_2$ and C, as well as Fe as an artifact of steel substrate (F 51–73.5 %; Ti 8–12.5 %; O 15.5–21.0 %; C 1.7–4.0 %; Fe 3.0–9.0 %). The average values of the main matrix components are the following: F 62.75 %; Ti 10.25 %; O 18.25 %; Fe 6 %; C 2.85 %. A background C signal does not allow to distinguish CNT, SiC, h-BN and P.

It can be seen from the Fig. 6, *c*–*e*, that addition of other additives (together with CNT) leads to increase of the number of dark particles. Critical rise of carbon content (41.42 % F; 23.33 % O; 20.16 % Fe; 8.76 % C; 6.33 % Ti) is observed in the dark particle (see Fig. 6, *f*), thereby it is presented supposedly CNT agglomerate saturated by carbon. High oxygen content can testify on presence of functional groups on CNT surface, while Fe can be a catalyst residual of CNT rise. Light particles of the white pigment $TiO_2$ are enriched by Ti and O, while fluorine and carbon are related to the surrounding matrix (F 54.36 %; Ti 26.08 %; O 17.63 %; Fe 1.6 %; C 1.93 %). The particles of $TiO_2$ pigment are distributed in a polymeric matrix in relatively uniform mode, while CNT can form local agglomerates (see Fig. 6, *f*). Analysis of SEM images allowed

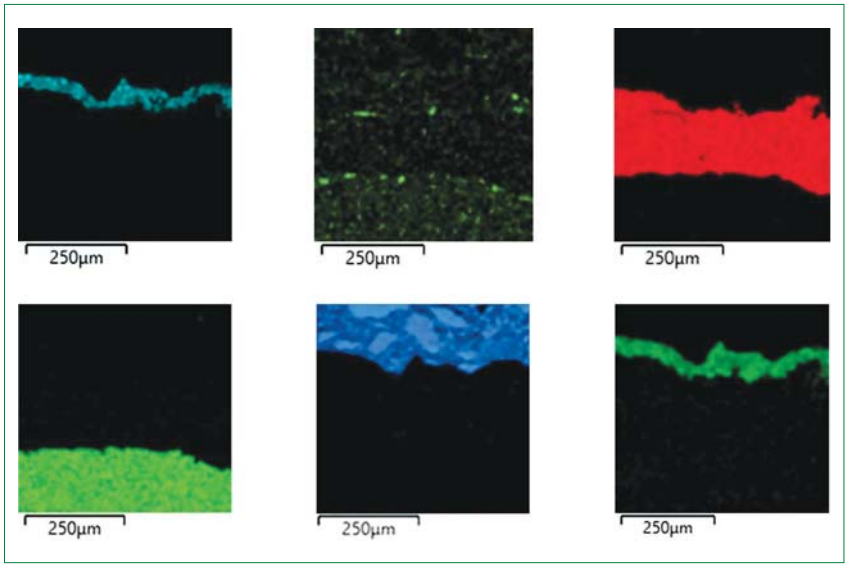


**Fig. 5. Distribution chart for the elements: *a*) fluorine F (Kα1,2); *b*) oxygen O (Kα1); *c*) aluminium Al (Kα1); *d*) ferrum Fe (Kα1); *e*) carbon C (Kα1,2); *f*) titanium Ti (Kα1)**

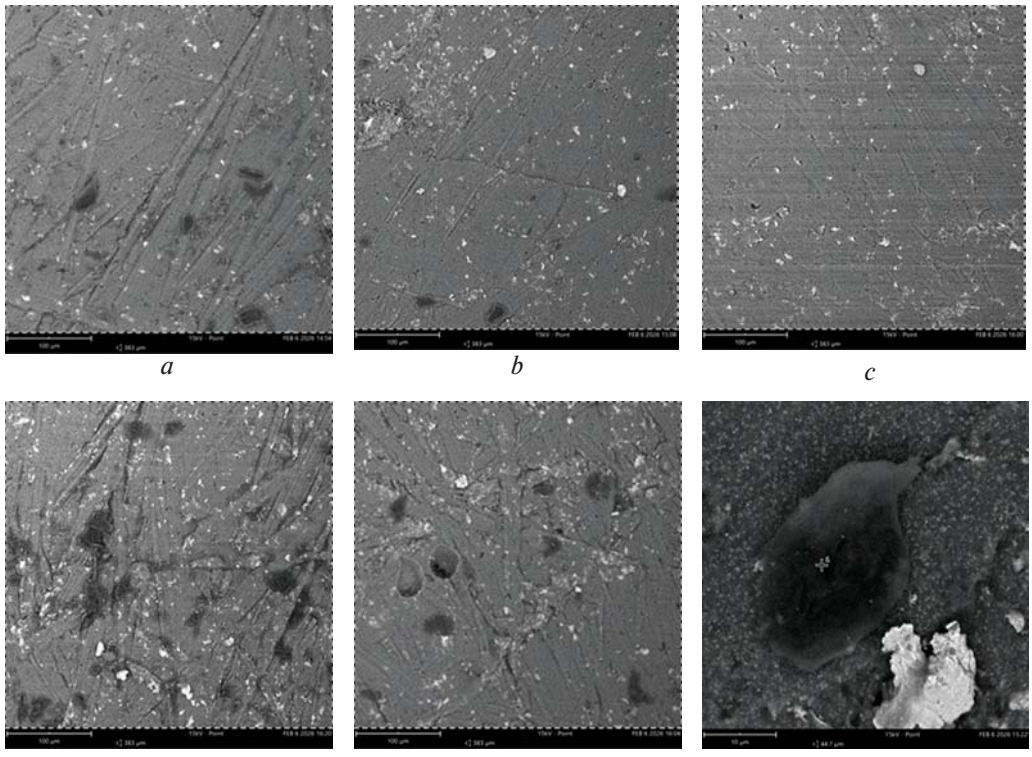

**Fig. 6. Structures of fluoroplastic coatings with nano-additives before (*a*) and after (*b–f*) additional ultrasonic treatment:** *a*) CNT; *b*) CNT (ultrasonic treatment); *c*) CNT+SiC; *d*) CNT+h-BN; *e*) CNT+SiC+h-BN; *f*) carbon agglomerate

to establish that providing additional ultrasonic treatment [40] makes it possible to decrease carbon agglomeration in compositions with CNT (see Fig. 6, *a–b*); their number is minimal in presence of SiC (see Fig. 6, *c*), what testifies on suppression of agglomeration process. Introduction of h-BN leads to increase of number and sizes of dark agglomerates (see Fig. 6, *d–e*), what can be connected with excessive number of CNT and their interaction with h-BN, with forming 3D net of hetero-agglomerates [41]. Such agglomerates can serve as serve concentrators and defects, where hydrogen diffusion can be accelerated. Though carbon agglomerate itself is a barrier, the separating boundary "agglomerate-matrix" remains potentially penetrating.

Thus, structure images of coatings (see Fig. 6) allow providing high-quality links between the type of nano-modifier having a tendency to agglomeration, presence of defects and increased coating permeability. The obtained conclusions agree with qualitative data of water permeability electrochemical measurements. To provide indirect assessment of presence of defects in coatings, the relationship between the coefficients of diffusion and flow reducing $\eta_J / \eta_D$ can be used; in this relationship $\eta_D$ characterizes the barrier effect from nano-particles and uniformity of their distribution, while $\eta_J$ is sensitive to penetration defects, because flow through a defect is higher than that through a volume by a sequence higher (**Table 2**).

CNT and SiC combination with maximal correlation between diffusion and permeability reducing (0.97) is considered as the best one. SiC is distributed homogeneously in nano-size state, thereby it is not seen in EDS spectra. Covalent links Si-C hold CNT at the surface of SiC particles, preventing their agglomeration (see Fig. 6, *c*). The presented results correlate with SEM which testify that part of CNT is agglomerated (see Fig. 6, *a–b*), thus compositions containing CNT

**Table 2. Effectiveness assessment of protective properties for coatings with nano-modifiers**

| Состав покрытия | $h_{CO}$, μm | $h_s$, μm | $D_{eff} \times 10^6$, cm²/s | $J(t) \times 10^{12}$, mol/(s·cm²) | *DRF* | *JRF* | $\eta_D$, % | $\eta_J$, % | $\eta_J / \eta_D$ |
|---|---|---|---|---|---|---|---|---|---|
| CNT +SiC+BN | 105 | 3094 | 0.16 | 3.37 | 11.21 | 2.51 | 91.08 | 60.2 | 0.66 |
| CNT +SiC | 84 | 3081 | 0.187 | 1.12 | 9.55 | 7.58 | 89.53 | 86.8 | 0.97 |
| CNT +BN | 81 | 3057 | 0.27 | 4.98 | 6.63 | 1.67 | 84.92 | 40 | 0.47 |
| CNT | 84 | 3058 | 0.235 | 1.79 | 7.61 | 4.80 | 86.86 | 79.2 | 0.91 |
| Al+AlOOH+CNT+SiC+BN | 220 | 3054 | 0.05 | 3.06 | 35.80 | 2.79 | 97.21 | 64.2 | 0.66 |
| Al+AlOOH+_CNT +SiC | 246 | 3072 | 0.06 | 0.91 | 29.83 | 9.33 | 96.65 | 89.3 | 0.92 |
| Al+AlOOH+_CNT +BN | 257 | 3049 | 0.09 | 3.83 | 19.89 | 2.23 | 94.97 | 55.2 | 0.58 |
| Al+AlOOH+_CNT | 244 | 3061 | 0.07 | 1.49 | 25.57 | 5.72 | 96.09 | 82.5 | 0.86 |

provide high (but not maximal) reducing of diffusion and permeability coefficients (0.91). h-BN is not detected in EDS spectra, because B and N are light elements, but compositions containing h-BN display the worse results of water permeability $\eta_J/\eta_D$ (0.47). h-BN is also dispersed badly, with forming large hetero-agglomerates with CNT (see Fig. 6, *d–e*); these agglomerates are characterized by creating microcracks and caverns around them during coating curing. It is caused by the fact that polymeric matrix can't moisture complicated rough surface of agglomerate. These caverns become channels for quick hydrogen diffusion with reducing $\eta_J$ to 40 %. SiC in the mixture CNT+SiC+BN increases $\eta_J/\eta_D$ (0.66) owing to fixing of nanotubes on their surface and reducing their agglomeration with h-BN. Phosphorus also was not found in EDS spectra in photoinitiator composition (which is based on phosphine oxide 819 (0.5 %)), due to its small weight and low content. Thereby we can evaluate about its distribution in coating only in indirect mode, via uniformity of their joint.

The adhesive layer Al+AlOOH increases adhesion of fluoroplastic coating with a steel substrate and barrier properties of metal polymeric coating; it also reduces its permeability for all compositions, what leads to $\eta_D$ growth (to 97 %) and permeability $\eta_J$ (to 89 %). Regularities which were revealed for fluoroplastic compositions, are completely saved also for coatings with Al+AlOOH substrate. The better correlation of diffusion and flow reducing coefficients $\eta_J/\eta_D$ (0.92) and maximal defect structure were displayed by the composition CNT with SiC (with sublayer). CNT+BN (with sublayer) showed the worse correlation (0.58) and maximal defect structure due to h-BN agglomeration. SiC presence in a ternary mixture CNT+SiC+BN (with sublayer) improves $\eta_J/\eta_D$ in comparison with h-BN (0.66), but it can't suppress completely agglomeration which was initiated by SiC.

## Conclusion

Difference in the effectiveness of permeability reducing between the coatings (52.1 % → 68.8 % → 77.1 %) displays that multi-layered composite systems with a combination of metallic and polymeric layers exceed substantially simple graphite and modified fluoroplastic coatings. It is expedient to use coatings with the effectiveness of permeability reducing not lower than 75 % for the steel 20 (which is sensitive for hydrogen embrittlement), as in the proposed polymer-composite coating, especially at high hydrogen pressure and durable operation. Effectiveness of diffusion reducing is 57.4 % for modified fluoroplastic coating and 67 % for graphite coating. The difference 10 % is explained by better barrier structure and higher adhesion of the graphite coating to steel 20. The composite coating Al+AlOOH+MFPE+graphite ($\eta_D$ = 87.7 %) demonstrates very high effectiveness of hydrogen diffusion reducing. It is explained by multi-layered structure of coating, high adhesion and CNT barrier properties. Such coating can be considered as a suitable barrier for typical operating conditions during hydrogen transportation and storage: high hydrogen pressure, long-time operation, increased requirements to resistance to hydrogen embrittlement.

Improvement of dispersion of nano-additives in fluoroplastic coatings and their layer-by-layer UV curing allowed increasing the coefficients of diffusion reducing to ~ 97 % and flow reducing to ~ 89 %. The type of nano-additives (CNT, SiC and h-BN), as well as uniformity of their distribution and sensitivity to agglomeration have a decisive influence on protective properties and defect structure of a fluoroplastic layer. The adhesive layer Al+AlOOH increases adhesion of a fluoroplastic layer to a steel substrate and additionally reduces diffusion and permeability for all compositions. CNt and SiC combination with maximal correlation between the coefficients of diffusion and permeability reducing (0.97) is the best one, due to homogenous distribution of nano-sized silicon carbide in a polymer matrix and its chemical interaction with CNT, which prevents their agglomeration.

## REFERENCES


1. Zhdaneev O. V. Providing technological sovereignty of the fuel and energy complex of Russian Federation. *Zapiski Gornogo instituta.* 2022. Vol. 258. pp. 1061–1070. DOI: 10.31897/PMI.2022.107.
2. Shammazov I. A., Borisov A. V., Aleksandruk B. S., Lopatenko G. V., Nikitina V. Algorithmic Models for Determining the Flow Patterns of Oil Pipelines in Gravity Sections. *International Journal of Engineering, Transactions A: Basics.* 2025. Vol. 38 (10). pp. 2476–2485. DOI: 10.5829/ije.2025.38.10a.22.
3. Shammazov I. A., Borisov A. V., Aleksandruk B. S. et al. Features of the effect of complicated mining conditions for construction and operation of self-flowing setions of pipeline transport. *Bezopasnost truda v promyshlennosti.* 2025. No. 7. pp. 39–43. DOI: 10.24000/0409-2961-2025-7-39-43.
4. Ermakov B. S., Ermakov S. B., Vologzhanina S. A., Khuznakhmetov R. M. Relationship between operating conditions and the emergence of nano- and ultradispersed grain boundary defects in weld joints. *Tsvetnye metally.* 2023. No. 8. pp. 80–85.
5. Litvinenko V. S., Tsvetkov P. S., Dvoinikov M. V., Buslaev G. V. Barriers of realizing hydrogen initiatives in the context of sustainable development of global power engineering. *Zapiski Gornogo instituta.* 2020. Vol. 244. pp. 428–438. DOI: 10.31897/pmi.2020.4.5.
6. Zagashvili Y., Kuzmin A., Buslaev G. et al. Small-scaled production of blue hydrogen with reduced carbon footprint. *Energies.* 2021. Vol. 14. No. 16. p. 5194. DOI: 10.3390/en14165194.
7. Nechaev Y. S. Metallic materials for the hydrogen energy industry and main gas pipelines: complex physical problems of aging, embrittlement, and failure. *Physics-Uspekhi.* 2008. Vol. 51 (7). p. 681. DOI: 10.1070/PU2008v051n07ABEH006570.
8. Li X. et al. Review of hydrogen embrittlement effect on fracture toughness of metallic materials: Influencing factors, and predictive models. *Engineering Fracture Mechanics.* 2025. p. 111392. DOI: 10.1016/j.engfracmech.2025.111392.
9. Xing X., Cheng R., Cui G., et al. Quantification of the temperature threshold of hydrogen embrittlement in X90 pipeline steel. *Materials Science and Engineering: A.* 2021. Vol. 800. p. 140118. DOI: 10.1016/j.msea.2020.140118.
10. Bolobov V. I., Tsvetkov A. S., Popov G. G., Dagaev S. E., Salnikov D. R., Tigranyan G. A. Comparison of Existing Methods for Studying Compatibility of Pipeline Steels with Compressed Hydrogen. *International Journal of Engineering, Transactions A: Basics.* 2026. Vol. 39 (04). pp. 917–924. DOI: 10.5829/IJE.2026.39.04A.10.
11. Bolobov V. I., Zhukov V. S., Tsvetkov A. S., Tigranyan G. A., Kondratieva V. M. Using the magnetic anisotropy method to determine the boundaries of stress-corrosion failure and prevent hydrogen damage to pipe steels. *Chernye metally.* 2025. No. 4. pp. 55–61.
12. Hu S. et al. A quantification study of hydrogen-induced cohesion reduction at the atomic scale. *Materials & Design.* 2022. Vol. 218. p. 110702. DOI: 10.1016/j.matdes.2022.110702.

13. Mansilla G., Hereñú S., Brandaleze E. Hydrogen effects on low cycle fatigue of high strength steels. *Materials Science and Technology*. 2014. Vol. 30 (4). pp. 501–505. DOI: 10.1179/1743284713Y.0000000328.
14. Borodin V. I. et al. Application of the Electrochemical Permeation Method for Hydrogen Diffusion Coefficient Determination in Pipeline Steel 10G2. *Coatings*. 2021. Vol. 11 (10). p. 1260. DOI: 10.3390/coatings11101260.
15. Jack T. A. et al. Investigation of the hydrogen induced cracking behaviour of API 5L X65 pipeline steel. *International Journal of Hydrogen Energy*. 2020. Vol. 45 (35). pp. 17671–17684. DOI: 10.1016/j.ijhydene.2020.04.211.
16. Thomas A., Szpunar J. A. Visualisation of diffusion sites and measurement of hydrogen traps in hot-rolled pipes. *Materials Science and Technology*. 2020. Vol. 36 (17). pp. 1870–1882. DOI: 10.1080/02670836.2020.1839205.
17. Xiao S. et al. Hydrogen permeation barriers and preparation techniques: A review. *Journal of Vacuum Science & Technology A*. 2022. Vol. 40 (6). p. 060803. DOI: 10.1116/6.0002178.
18. Henager C. H. Hydrogen permeation barrier coatings. *Materials for the hydrogen economy*. 2007. pp. 181–190. DOI: 10.1201/9781420006070.
19. Samanta S. et al. Development of amorphous Ni-P coating over API X70 steel for hydrogen barrier application. *Surface and Coatings Technology*. 2020. Vol. 403. p. 126356. DOI: 10.1016/j.surfcoat.2020.126356.
20. Kapuscinsky N. et al. Polymeric Coatings for Preventing Hydrogen Embrittlement in Industrial Storage and Transmission Systems. *ACS Applied Engineering Materials*. 2024. Vol. 2 (11). pp. 2488–2503. DOI: 10.1021/acsaenm.4c00367.
21. Petkova A. P., Pryakhin E. I., Zlotin V. A., Gareev D. V. Comparative analysis of effectiveness of hydrogen permeability reducing via using protective coatings during its transportation, storage and production. *Dizain. Materialy. Tekhnologiya*. 2024. Vol. 4 (76). pp. 167–174. DOI: 10.46418/1990-8997_2024_4(76)_167_174.
22. de Souza Brandolt C. et al. Determination of hydrogen trapping mechanisms by microprinting in Ni and Co coatings obtained by HVOF. *Surface and Coatings Technology*. 2019. Vol. 362. pp. 262–273. DOI: 10.1016/j.surfcoat.2019.01.111. 23.
23. Wetegrove M. et al. Preventing hydrogen embrittlement: the role of barrier coatings for the hydrogen economy. *Hydrogen*. 2023. Vol. 4 (2). pp. 307–322. DOI: 10.3390/hydrogen4020022.
24. Sivenkov A. V., Konchus D. A., Gareev D. V., Pryakhin E. I. Application of Cr–Ni coatings by chemical-thermal treatment from lowmelting metal solutions. *Chernye metally*. 2024. No. 12. pp. 101–106.
25. Pryakhin E. I., Pribytkova D. A. Development and application of a complex polymer coating to ensure high corrosion resistance of the outer surface of steel pipes of urban heating networks. *CIS Iron and Steel Review*. 2025. Vol. 29. pp. 97–101.
26. Pryakhin E. I., Azarov V. A. Study of protective properties of fluoroplastic polymer compositions on steel samples with the aim of their potential use for internal coatings of main gas pipelines. *Chernye metally*. 2025. No.4. pp. 62–66.
27. Pauly S. Permeability and diffusion data. *Polymer handbook*. 1999. Vol. 2. VI/551. DOI: 10.1002/0471532053.
28. Aman M. M., Mohammed B. S., Al-Yacouby A. M. Hydrogen Permeation Resistance of PVDF–Graphene Nanocomposite Coatings for Metallic Pipelines. *Polymers*. 2025. Vol. 17 (16). p. 2262. DOI: 10.3390/polym17162262.
29. Yuan S. et al. A bi-layer orientated and functionalized graphene-based composite coating with unique hydrogen gas barrier and long-term anti-corrosion performance. *Carbon*. 2023. Vol. 205. pp. 54–68. DOI: 10.1016/j.carbon.2023.01.027.
30. Guo H. X. et al. Enhanced anti-corrosion and hydrogen resistance performance for epoxy resin composite coating with modified boron nitride. *International Journal of Hydrogen Energy*. 2025. Vol. 141. pp. 35–45. DOI: 10.1016/j.ijhydene.2025.05.335.
31. Kumar S. et al. Enhancement of hydrogen gas permeability in electrically aligned MWCNT-PMMA composite membranes. *Micron*. 2010. Vol. 41. No. 7. pp. 909–914. DOI: 10.1016/j.micron.2010.05.016.
32. Nikolaychik A. V. et al. Influence of carbon nanomodifiers on the properties of paint and lacquer materials and coatings. *Vesnik Vitsebskaga dzyarzhaunaga universiteta*. 2010. No. 3. pp. 34–42.
33. Kurihara K., Serizawa A. Formation Mechanism of Two-Layered AlO (OH) Films on Aluminum Alloys via the Steam Coating Process. *Advanced Materials Interfaces*. 2025. pp. e00304. DOI: 10.1002/admi.202500304.
34. Jones R. H., Thomas G. J. Materials for the hydrogen economy. CRC Press. 2007. p. 352. DOI: 10.1201/9781420006070.
35. Tan X., Wan X. Hydrogen permeation behavior in $Fe_3Al$-based alloy. *Journal of Shanghai University (English Edition)*. 2000. Vol. 4 (3). pp. 250–253. DOI: 10.1007/s11741-000-0073-2.
36. Pisarev A. A., Tsvetkov I. V., Marenkov E. D., Yarko S. S. Hydrogen permeability through metals. *Proceedings of the Fifth International conference and Ninth International school of young scientists and specialists named after Kurdyumov A. A.* 2014. Vol. 1. pp. 155–176.
37. Reddy K. S., Govindaraj Y., Neelakantan L. Hydrogen diffusion kinetics in dual-phase (DP 980) steel: The role of pre-strain and tensile stress. *Electrochimica Acta*. 2023. Vol. 439. p. 141727. DOI: 10.1016/j.electacta.2022.141727.
38. Mohtadi-Bonab M. A., Masoumi M. Different aspects of hydrogen diffusion behavior in pipeline steel. *Journal of Materials Research and Technology*. 2023. Vol. 24. pp. 4762–4783. DOI: 10.1016/j.jmrt.2023.04.026.
39. Liu L. et al. Fabrication and hydrogen permeation resistance of dense CrN coatings. *Surface and Coatings Technology*. 2022. Vol. 437. p. 128326. DOI: 10.1016/j.surfcoat.2022.128326.
40. Akopov F. A. et al. SiC-based composite ceramics alloyed by carbon nanotubes. *Vestnik Obyedinennogo instituta vysokikh temperatur*. 2018. Vol. 1. No. 1. pp.51–55. DOI: 10.33849/2018112.
41. Su Z. et al. Anisotropic thermally conductive flexible polymer composites filled with hexagonal born nitride (h-BN) platelets and ammine carbon nanotubes ($CNT–NH_2$): Effects of the filler distribution and orientation. *Composites Part A: Applied Science and Manufacturing*. 2018. Vol. 109. pp. 402–412. DOI: 10.1016/j.compositesa.2018.03.021.